ADVANCED FUNCTIONAL MATERIALS
www.afm-journal.de

Materials Views
www.MaterialsViews.com

# Influence of Molecular Weight on the Performance of Organic Solar Cells Based on a Fluorene Derivative

By *Christian Müller,* Ergang Wang, L. Mattias Andersson, Kristofer Tvingstedt, Yi Zhou, Mats R. Andersson,* and *Olle Inganäs*

**The performance of organic photovoltaic (OPV) bulk-heterojunction blends comprising a liquid-crystalline fluorene derivative and a small-molecular fullerene is found to increase asymptotically with the degree of polymerization of the former. Similar to various thermodynamic transition temperatures as well as the light absorbance of the fluorene moiety, the photocurrent extracted from OPV devices is found to strongly vary with increasing oligomer size up to a number average molecular weight, $M_n \approx 10\,kg\,mol^{-1}$, but is rendered less chain-length dependent for higher $M_n$ as the fluorene derivative gradually adopts polymeric behavior.**

## 1. Introduction

Interest in fluorene-based organic semiconductors has surged thanks to their ability to display high levels of (polarized) photo- and electroluminescence as well as useful electronic charge-transport properties.[1–3] More recently, a promising photovoltaic performance has been achieved through incorporation of such compounds in bulk-heterojunction blends.[4–7]

Both, oligo- and polyfluorene derivatives have been studied extensively and predominantly the latter have been found to display superior characteristics, such as significantly improved opto-electronic behavior (e.g., field-effect mobility, photoluminescence, circular dichroism, and photovoltaic performance),[8–11] as well as, for instance, the ability to form oriented fibers.[12–14] Generally, one would expect that with increasing chain length most properties become less affected by small variations in the degree of polymerization, as indeed observed for the field-effect mobility, photoluminescence, as well as transition temperatures of various polyfluorenes.[9,14] However, frequently, it has been found that the viscosity of high molecular weight materials can limit their processability, which in some cases had an adverse effect on, for example, the molecular ordering achievable with those species.[10,15,16] More advanced fluorene derivatives, such as some of those recently developed for organic photovoltaic (OPV) applications,[6,7] suffer, in addition, from the limited solubility of higher molecular weight fractions in common organic solvents, which further complicates their synthesis as well as processability. Thus, in order to permit an attractive (photovoltaic) performance whilst retaining good solution processability of these semiconductors, it may be necessary to compromise between underperforming but readily soluble oligomeric species and opto-electronically superior but less tractable polymers.

Here, we explore the influence of molecular weight on various optical and physico-chemical properties of poly[2,7-(9,9-dioctyl-fluorene)-alt-5,5-(4′,7′-di-2-thienyl-2′,1′,3′-benzothiadiazole)] (commonly abbreviated as APFO-*3* or PFDTBT, with "P" denoting *poly*, but here as F8TBT in order to refer to both an oligo- and polymeric material), as those can be readily related to the chain conformation. This we compare with the OPV performance of blends with the small-molecular electron-acceptor [6,6]-phenyl-$C_{61}$-butyric acid methyl ester ($PC_{61}BM$). In particular, we find that with increasing molecular weight of F8TBT the photovoltaic characteristics improve and eventually become less sensitive to small changes in the degree of polymerization, offering a window in terms of good processability as well as functionality.

## 2. Results and Discussion

To gain initial insight into the molecular conformation of F8TBT, in a first set of experiments we investigated the intrinsic viscosity, $[\eta]$, of four representative batches, that is, **1**, **3**, **8**, and **11** (see Table 1 for molecular weights), dissolved in *ortho*-dichlorobenzene (*o*DCB). Polymeric F8TBT should obey the Mark–Houwink–Sakurada equation $[\eta] = K \cdot M_n^{\alpha}$, which relates $[\eta]$ and the number-average molecular weight, $M_n$, where $K$ and $\alpha$ are constants.[17] However, in the log–log plot displayed in Figure 1, $[\eta]$ doesn't follow a simple linear trend with respect to $M_n$ but displays a concave tendency, suggesting that shorter, oligomeric species are of more rigid nature.[18] At higher $M_n$, the slope and hence the exponent $\alpha$ approach ~0.8, indicating that F8TBT molecules of sufficient chain length adopt a flexible to semi-flexible conformation in *o*DCB.

[*] Dr. C. Müller, Dr. L. M. Andersson, Dr. K. Tvingstedt, Dr. Y. Zhou, Prof. O. Inganäs
Department of Physics, Chemistry & Biology
Linköping University
58183 Linköping (Sweden)
E-mail: christian.muller@ifm.liu.se
Dr. E. Wang, Prof. M. R. Andersson
Department of Chemical and Biological Engineering
Chalmers University of Technology
41296 Göteborg (Sweden)

DOI: 10.1002/adfm.201000224

**Table 1.** $M_n$ and $M_w$ of F8TBT batches **1**–**14**, relative to polystyrene standards; polydispersity index, p.d.i.; degree of polymerization, d.p. $= M_n/M_0$, where $M_0 = 686\,g\,mol^{-1}$ is the molecular weight of a F8TBT repeat unit.

| F8TBT batch | $M_n$ [kg mol$^{-1}$] | $M_w$ [kg mol$^{-1}$] | p.d.i. | d.p. |
|---|---|---|---|---|
| **1** | 2 | 3 | 1.5 | 3 |
| **2** | 4 | 6 | 1.5 | 6 |
| **3** | 5 | 8 | 1.6 | 7 |
| **4** | 5 | 12 | 2.4 | 7 |
| **5** | 6 | 14 | 2.3 | 9 |
| **6** | 7 | 12 | 1.7 | 10 |
| **7** | 7 | 13 | 1.9 | 10 |
| **8** | 7 | 14 | 2.0 | 10 |
| **9** | 8 | 14 | 1.8 | 12 |
| **10** | 15 | 24 | 1.6 | 22 |
| **11** | 18 | 32 | 1.8 | 26 |
| **12** | 30 | 45 | 1.5 | 44 |
| **13** | 36 | 65 | 1.8 | 52 |
| **14** | 38 | 69 | 1.8 | 55 |

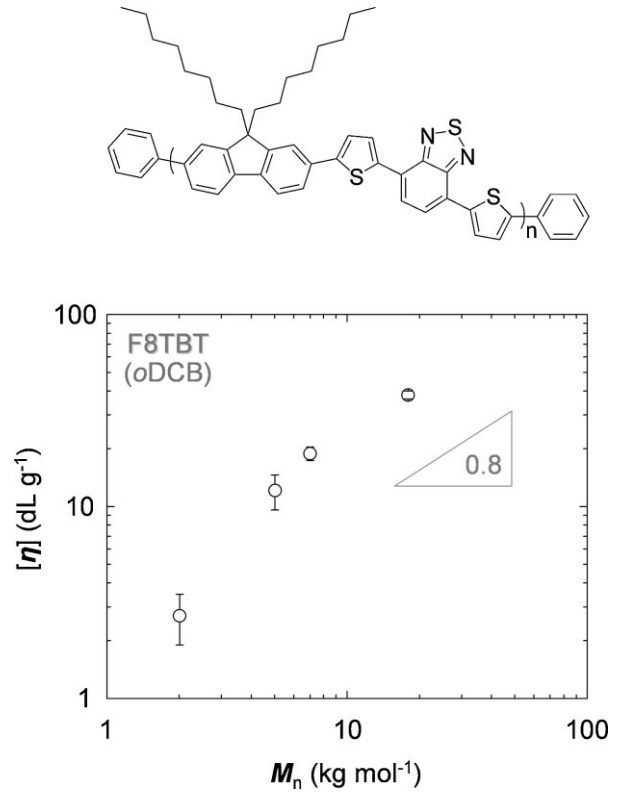


**Figure 1.** Chemical structure of F8TBT (top) and Mark–Houwink–Sakurada plot of [$\eta$] with respect to $M_n$ of **1**, **3**, **8**, and **11** in *o*DCB (bottom). Unfortunately, the limited availability of the remaining batches prevented us from conducting a more complete study. A Mark–Houwink–Sakurada exponent of $\alpha = 0.8$ is indicated (generally, $\alpha \approx 0.5$–$0.8$ for flexible polymers; $\alpha > 0.8$ for semi-flexible polymers; $\alpha = 2$ if the species is a perfectly stiff rod) [17]. Error bars represent the uncertainty in [$\eta$] as extrapolated from dilution series.

The semi-flexible character of F8TBT is corroborated by the appearance of liquid-crystalline textures in thin films that were solidified by cooling from 300 °C to ambient as illustrated by a series of polarized optical micrographs depicted in Figure 2.[7] It is worth noting that the observed domain size of such processed F8TBT decreases considerably for **12**–**14**, implying entanglement of polymer chains and, thus, we infer an entanglement molecular weight, $M_e \approx 18$–$30\,kg\,mol^{-1}$.[19]

In order to further elucidate the transition of rigid short-chain oligomers to more random-coil semi-flexible polymers, we deduced the glass and liquid-crystalline/isotropic transition temperatures, $T_g$ and $T_{lc/i}$, of **1**–**14** by means of differential scanning calorimetry (DSC) and polarized optical microscopy (Fig. 3). The heat stability of F8TBT up to ~320 °C was confirmed by thermal gravimetric analysis (TGA) measurements (not shown). Conspicuously, a more ordered crystalline phase—readily observed for many other fluorene-based polymers[3,9,10,13–16]—is absent for the present material. The Flory–Fox equation $T_g(M_n) = T_g(M_\infty) + B \cdot M_n^{-1}$, where $T_g(M_\infty)$ is the asymptotic value of $T_g$ at infinite $M_n$ and $B$ a constant,[20] was employed to describe the molecular weight dependence of $T_g$. For other materials systems a variety of characteristics, such as their tensile strength, $T_{lc/i}$ and the wavelength of maximum light absorbance,[21–23] have been demonstrated to follow a similar trend, although more accurate models can be developed.[23] Throughout this study, a simple $M_n^{-1}$ relation was successfully used to illustrate the dependence of various properties on $M_n$. It has been suggested that the Flory–Fox equation reflects a change in chain statistics due to a decreasing influence of the chain-end free volume and the development of a random-coil conformation with increasing molecular weight,[20,24] resulting in a largely chain-length independent behavior—particularly in absence of a crystalline phase. Accordingly, we find that the transition temperatures of F8TBT vary dramatically with molecular weight up to $M_n \approx 10\,kg\,mol^{-1}$. Thus, it appears reasonable to consider F8TBT as oligomeric below and as more polymeric (macromolecular) above this threshold, as F8TBT gradually adopts a random-coil and eventually entangled chain configuration (i.e., for $M_n > M_e$).[24–27]

A change in chain conformation can be expected to drastically influence the optical properties of an organic semiconductor as its delocalized electronic transition states are related to the average conjugation length along the backbone of the molecule, which, in addition, may be constrained by the presence of chain ends, as demonstrated for a variety of oligomer systems based on, for example, paraphenylenevinylene[23,28] or 9,9-dihexylfluorene.[29] F8TBT features two absorbance bands: a blue band below 400 nm attributed to a fully delocalized excitonic $\pi$–$\pi^*$ transition and a red band around 550 nm that has been ascribed to a localized charge-transfer state with the excited electron confined to the benzothiadiazole acceptor (B), whereas the corresponding hole remains delocalized across fluorene (F8) and thiophene (T) units along the $\pi$-conjugated backbone.[30] Delocalization of these transition states is prone to increase with oligomer size until the chain adopts a semi-flexible conformation. Hence, we find that both absorbance bands significantly red-shift with increasing oligomer molecular weight but saturate for higher degrees of polymerization (Fig. 4), confirming that F8TBT approaches macromolecular behavior for $M_n > 10\,kg\,mol^{-1}$. [Note that a similar behavior has been reported for thin films of poly[2-methoxy-5-(2′-ethylhexyloxy)-

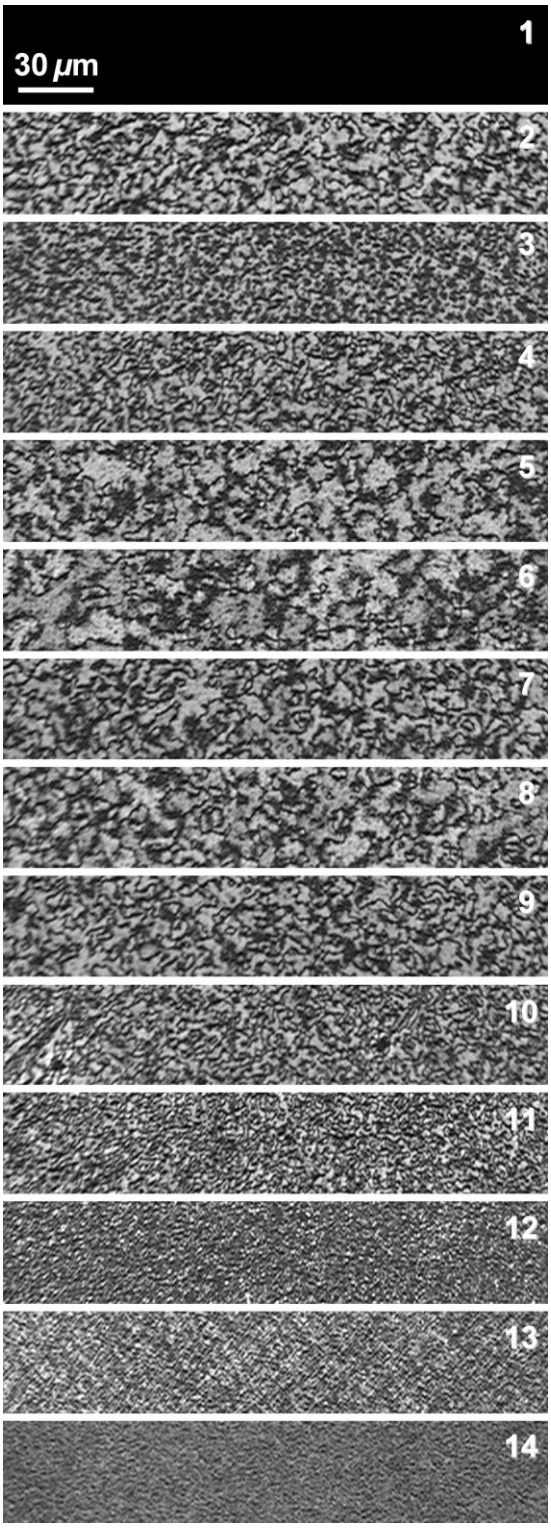


**Figure 2.** Polarized optical micrographs of F8TBT films solidified by cooling from 300 °C to ambient, that is, from $T > T_{lc/i}$ to room temperature. Note that **1** does not display a liquid-crystalline texture.

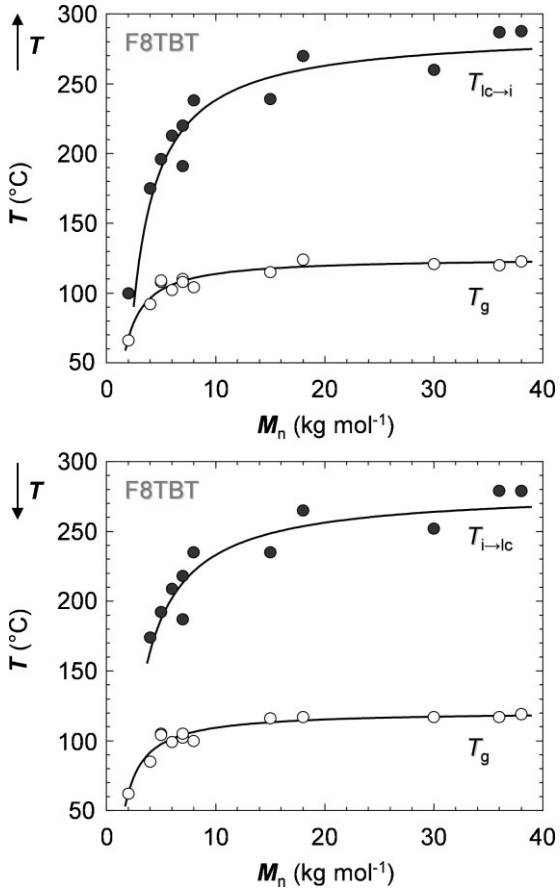


**Figure 3.** $T_g$ (open circles) and $T_{lc/i}$, that is, $T_{lc\rightarrow i}$ and $T_{i\rightarrow lc}$, (full circles) versus $M_n$ of **1**–**14** deduced from DSC second heating (top) and cooling thermograms (bottom). $T_{lc/i}$ were confirmed optically; **1** was found to be monotropic as a liquid-crystalline phase was only observed during heating. Trendlines were constructed assuming a $M_n^{-1}$ relation (i.e., the Flory–Fox equation for $T_g$).

1,4-phenylenevinylene] (MEH-PPV), for which, in addition, preferential in-plane orientation of chain segments was observed for high molecular-weight polymers.[31]] Interestingly, the red-shift in the absorbance maximum of F8TBT dissolved in *o*DCB and of F8TBT solidified in the presence of an excess $PC_{61}BM$ fraction (i.e., 20:80 F8TBT:$PC_{61}BM$) follows a comparable trend (Fig 4b), whereas the peak absorbance wavelengths, $\lambda_p$, of spin-coated and heat-treated F8TBT thin films saturate at a somewhat lower molecular weight (Fig. 4c and d). Thus, the precise environment appears to affect the chain flexibility of F8TBT (the value of $M_n$, for which $\lambda_p$ saturates, can be taken as a measure for the effective conjugation length)[23] and in the case of the OPV blends discussed below the material can be considered as highly "diluted."

In order to relate the above observations to the OPV performance of bulk-heterojunction blends comprising the present F8TBT oligomers and polymers, we fabricated a series of solar cells based on **1**–**14**. The active layers of these devices comprised 80 wt% of the electron acceptor $PC_{61}BM$—a composition that has been reported to yield optimum power conversion[32]—and were spin-coated from *o*DCB.

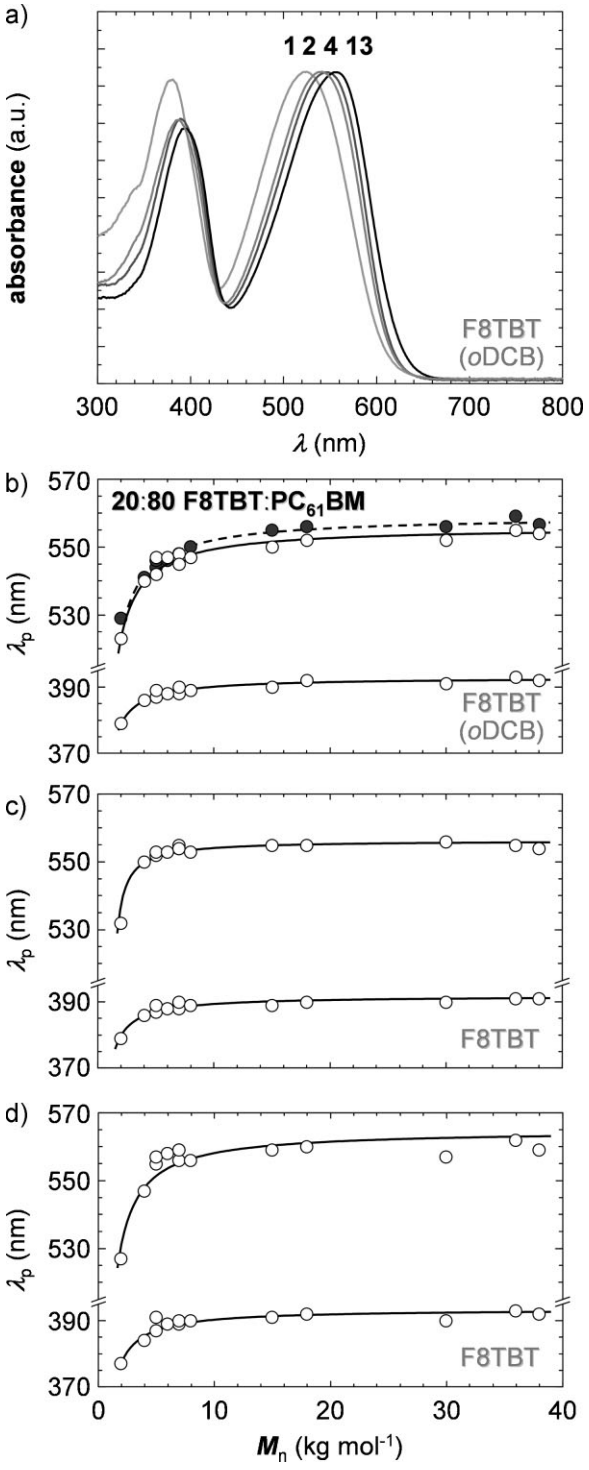


**Figure 4.** a) Normalized UV-vis absorbance spectra of **1**, **2**, **4**, and **13** dissolved in *o*DCB. b) Peak absorbance wavelengths, $\lambda_p$, versus $M_n$ of **1–14** in dilute *o*DCB solution as well as thin films of 20:80 F8TBT:$PC_{61}BM$ solidified, that is, spin-coated, from *o*DCB [note that the blue peak below 400 nm was overshadowed by the absorbance of $PC_{61}BM$]; c) thin films of F8TBT spin-coated from *o*DCB; d) and thin films of F8TBT solidified by cooling from 300 °C to ambient. Trendlines were constructed assuming a $M_n^{-1}$ relation.

Several reports have demonstrated that solidification of this materials combination from solutions with chlorinated benzenes yields a largely homogeneous mixture,[33–35] with phase separation limited to partial crystallization of the small-molecular $PC_{61}BM$, resulting in uniformly dispersed crystallites.[34,36] This is in contrast to solidification from other solvents such as chloroform, for which spinodal decomposition has been shown to precede vitrification of the blend, leading to a more inhomogeneous distribution of F8TBT;[34] an effect that may be more pronounced if higher molecular-weight polymers are employed. However, coarser F8TBT:$PC_{61}BM$ blends still feature significant intermixing on the molecular level, as evidenced by efficient photoluminescence quenching reported in previous studies.[37,38]

Nevertheless, here, F8TBT can be considered to be rather homogeneously distributed in a matrix of the small-molecular $PC_{61}BM$, corroborated by the smooth, featureless texture of thin films as revealed by a series of scanning force micrographs in Figure 5a. Despite the similar appearance of these blends, we find that their OPV performance was significantly affected by the particular choice of F8TBT batch (Fig. 5b). Whereas the open-

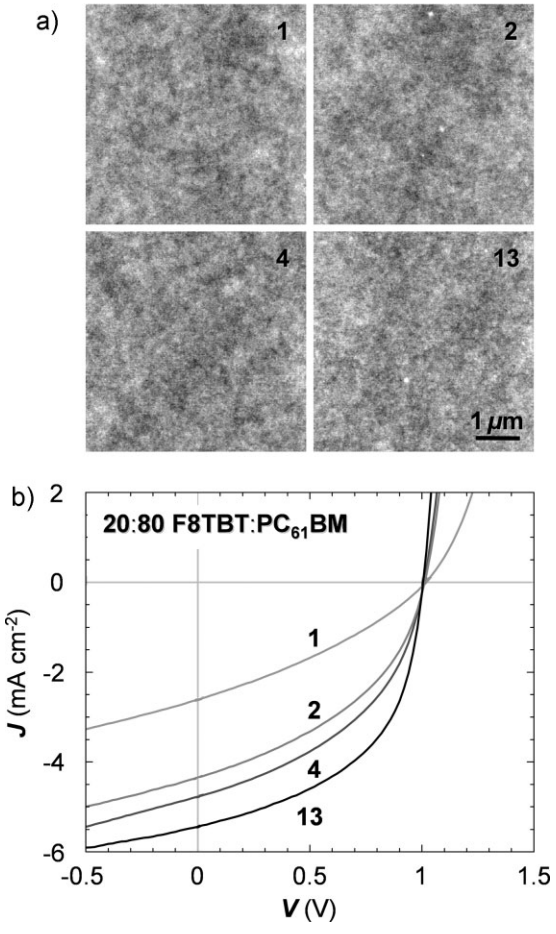


**Figure 5.** a) SFMs of 20:80 F8TBT:$PC_{61}BM$ thin films (z-range = 5 nm) comprising **1** (top left), **2** (top right), **4** (bottom left), and **13** (bottom right). b) Corresponding *J–V* characteristics of 20:80 F8TBT:$PC_{61}BM$ photovoltaic devices based on **1**, **2**, **4**, and **13** under 1000 W $m^{-2}$ illumination.

circuit voltage, $V_{oc}$, was found to slightly decrease with increasing molecular weight of F8TBT, especially the short-circuit current, $J_{sc}$, and to a limited extend also the fill factor, *FF*, were positively affected, overall resulting in a much enhanced power-conversion efficiency, *PCE* (Fig. 6). Similar to various properties of F8TBT that have been discussed above, such as $T_g$, $T_{lc/i}$, and the red-shift in absorbance, the characteristics of F8TBT:$PC_{61}BM$ photovoltaic devices are found to be proportional to $M_n^{-1}$ and to saturate for $M_n > 10\,kg\,mol^{-1}$, indicating the influence of related microstructural features, such as the number of F8TBT chain ends and the chain flexibility.

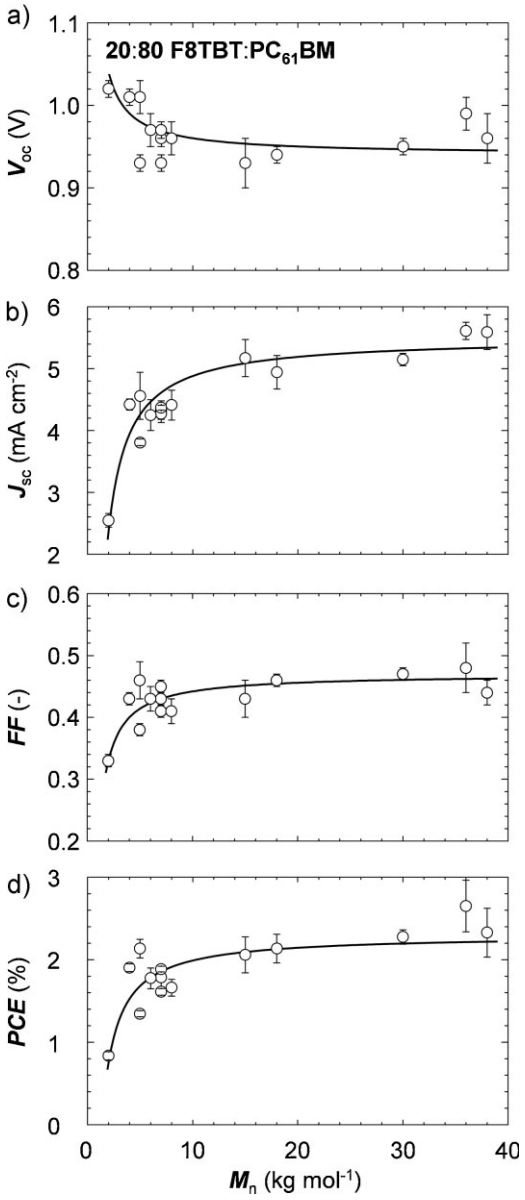


**Figure 6.** Average $V_{oc}$, $J_{sc}$, *FF*, and *PCE* versus $M_n$ of 20:80 F8TBT:$PC_{61}BM$ photovoltaic devices based on **1**–**14**. Trendlines for $V_{oc}$, $J_{sc}$, *FF* and *PCE* were constructed assuming a $M_n^{-1}$ relation. Error bars represent the standard deviation of solar cell characteristics based on comparison of similar devices.

The slight decrease in $V_{oc}$ can be rationalized by the red-shift in absorbance of F8TBT with increasing oligomer size, which is indicative of a change in energy levels with increasing chain length. As a result, the bandgap between the highest occupied molecular orbital (HOMO) of F8TBT and the lowest unoccupied molecular orbital (LUMO) of $PC_{61}BM$ will be reduced, leading to a decrease in photovoltage with increasing molecular weight up to $M_n \approx 10\,kg\,mol^{-1}$.[39,40]

Several factors may contribute towards the observed trend in photocurrent generation. Certainly, an improved overlap between the solar spectrum and F8TBT absorbance—red-shifting with increasing oligomer size—will enhance the number of absorbed photons,[11] virtually all of which will result in excitons that dissociate into a weakly bound electron–hole charge pair (charge-transfer state) located at the interface of the electron-donating (hole-conducting) F8TBT and electron-accepting (electron-conducting) $PC_{61}BM$.[41,42] However, a large fraction of charge pairs may never contribute to the extracted photocurrent because of excessive recombination, which can be of geminate (monomolecular) nature, referring to recombination of such a bound charge pair,[12,42–44] or of non-geminate (bimolecular) nature, referring to the recombination of free charges (i.e., free electrons and holes created by the complete dissociation of the bound charge pair) en route to the electrodes.[45,46]

Undoubtedly, charge pairs generated at isolated sites (e.g., chain ends)—a process that is more prevalent if short-chain oligomers are blended into the $PC_{61}BM$ matrix—will be strongly localized, which may prohibit efficient dissociation and, therefore, encourage their geminate recombination. In contrast, dissociation of bound electron–hole pairs generated in proximity to longer polymer chains may benefit from the more extended delocalization of holes along the conjugated backbone (i.e., a higher intra-chain hole mobility).[47] In addition, an increase in chain length and thus connectivity of the hole-transporting F8TBT can improve inter-chain hole transport and, thus, may to some extent discourage bimolecular recombination of dissociated charges (a process that cannot be neglected because of the insufficient phase separation of the present OPV blends).[48] Electron transport, however, may be less affected by changes in F8TBT molecular weight as the small-molecular electron-conductor $PC_{61}BM$ can be expected to efficiently percolate throughout the active layer by virtue of the large excess in volume fraction. The benefit of higher F8TBT molecular weight on hole transport is tentatively reflected in the somewhat improved fill factor of F8TBT:$PC_{61}BM$ photovoltaic devices and corroborated by the increase in blend hole mobility, $\mu_h$, that was extracted from field-effect transistor (FET) measurements (Fig. 7). Our FET devices did not display discernible electron transport, which we assign to electron mobilities, $\mu_e$, that are substantially lower than $\mu_h$, as confirmed in Ref. [32] using photo-charge extraction by linearly increasing voltage (photo-CELIV), a technique that for disordered systems can be correlated with FET measurements.[49] Unfortunately, we observed a pronounced spread in *FF* and $\mu_h$ for devices produced with F8TBT of similar $M_n \approx 4$–$8\,kg\,mol^{-1}$ (**2**–**9**), which to some extend may reflect yet unidentified differences in electronic purity between various F8TBT batches. Interestingly, we find that, generally, a higher $\mu_h$ results in an improved *FF*.

Thus, for the present system, the above arguments suggest an improvement in light absorbance and bound charge pair

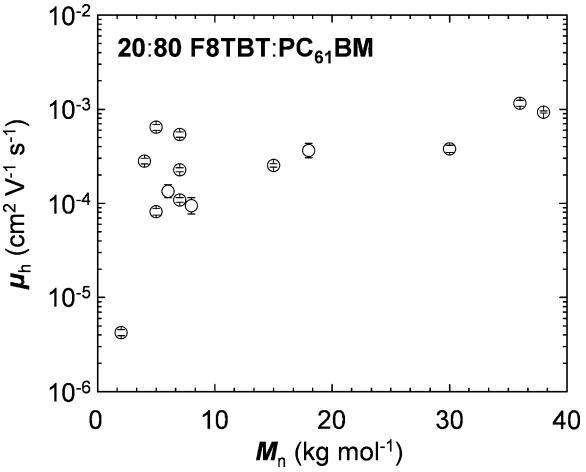


**Figure 7.** Average $\mu_h$ versus $M_n$ extracted from 20:80 F8TBT:$PC_{61}BM$ FETs based on **1**–**14**. Error bars represent the standard deviation of $\mu_h$ based on comparison of similar devices.

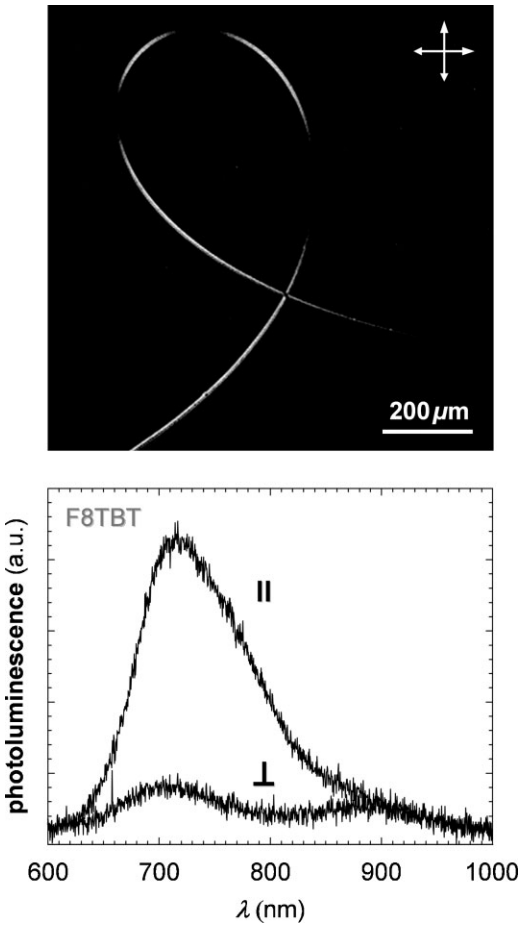


**Figure 8.** Polarized optical micrograph (top; orientation of polarizer and analyzer as indicated) and polarized photoluminescence spectrum (bottom) of a F8TBT fiber produced with **14** (orientation of the polarizer with respect to the fiber axis as indicated).

dissociation dynamics accompanied by reduced recombination losses as well as improved hole charge transport with increasing degree of polymerization of F8TBT, resulting in significantly enhanced photocurrent generation, which saturates for $M_n > 10\,kg\,mol^{-1}$ as F8TBT assumes polymeric behavior. Here, it is interesting to note that the molecular-weight dependence of the OPV performance of similar blends composed of a related fluorene derivative, which comprises didecyl instead of dioctyl side-chains (i.e., F10DTBT) and again $PC_{61}BM$, was recently explained principally on the basis of limited bound charge pair dissociation dynamics in low molecular-weight mixtures due to rapid geminate recombination.[11] Besides, the same process was also found to be central for the photo-physics of F8TBT($M_n \approx 5\,kg\,mol^{-1}$):$PC_{61}BM$ blends.[42]

Furthermore, it is important to note that for the range of $M_n$ investigated in the present study, F8TBT with $M_e \approx 18$–$30\,kg\,mol^{-1}$ is unlikely to be (strongly) entangled when diluted with $PC_{61}BM$. However, chain entanglement for $M_n >> M_e$ can affect the molecular order of the polymer,[10,15,16] and, hence, the OPV performance may eventually deviate from a simple asymptotic trend. Similar behavior has been reported for blends comprising the semicrystalline polymer poly(3-hexylthiophene) (P3HT) and $PC_{61}BM$, which displayed a decrease in photovoltaic performance when comprising P3HT of $M_n > 34\,kg\,mol^{-1}$, attributed to the negative effect of chain entanglement of higher molecular-weight P3HT on polymer crystallization.[50]

Finally, we would like to stress that any distinction between an oligomeric and polymeric regime is in fact strongly dependent on the particular property of interest. This is most evidently illustrated by the polarized optical micrograph of a birefringent fiber displayed in Figure 8 (top), a macroscopic structure, which could only be produced with the highest available molecular-weight F8TBT batch (**14**). Such fibers featured pronounced orientation of polymer chains, as confirmed by polarized emission spectroscopy (Fig. 8, bottom). Clearly, although not suitable for certain fabrication schemes that rely on solubilization in more benign organic solvents (c.f., Experimental), higher molecular weight polymers open processing routes and permit structures that are not readily accessible with oligomeric semiconductor species.

## 3. Conclusions

For the here discussed spin-coated bulk-heterojunction blends based on F8TBT and $PC_{61}BM$, it appears sufficient to employ relatively low molecular-weight polymers with $M_n > 10\,kg\,mol^{-1}$ in order to guarantee good solution processability as well as a satisfactory OPV performance. We argue that ensuring the polymeric nature of F8TBT is of benefit for light absorbance, charge dissociation as well as charge extraction, the relative importance of which is the subject of an ongoing investigation. Certainly, an asymptotic dependence on molecular weight can be expected for other non-crystalline polymer:fullerene OPV systems. Moreover, materials selection based on a simple oligomer/polymer argument may also be relevant for other opto-electronic applications comprising bulk-heterojunction blends, such as low dark-current photo-detectors and light-emitting transistors.

## 4. Experimental

*Materials*: F8TBT batches **1**–**14** were prepared according to previously reported procedures [6]; the molecular weight was controlled by varying the reaction time as well as by using an excess of the fluorene monomer, which, therefore, can be expected to preferentially flank the synthesized material at either chain end. The phenyl end-capped reaction product was carefully purified by dissolution in chloroform (**1**–**9**) or *o*DCB (**10**–**14**) and addition of concentrated ammonia; after stirring for 24h the organic phase was separated and washed three times with distilled water, followed by precipitation in methanol and finally collected by filtration. $PC_{61}BM$ was obtained from Solenne BV.

Chlorinated benzenes—although not benign organic solvents—were chosen as solvents throughout this study as they readily permitted dissolution of all available batches at ambient; in contrast to chloroform or toluene, for instance, which only dissolved lower molecular weight F8TBT.

*Molecular Weight Determination*: Number and weight average molecular weights, $M_n$ and $M_w$, of **1**–**14** were determined using size exclusion chromatography (SEC) on a Waters 150 CV equipped with at refractive index detector using 1,2,4-trichlorobenzene as solvent at 135 °C and are listed in Table 1. Calibration was performed with narrow molecular weight polystyrene standards.

*Viscometry*: Intrinsic viscosities were determined using an Ubbelohde viscometer from Schott (capillary number 0a). Dilution series with solutions of **1**, **3**, **8**, and **11** in *o*DCB (1–10 g $dL^{-1}$) were recorded with a Schott AVS 360 controller.

*Thermal Analysis*: TGA was conducted under nitrogen at a scan rate of 10 °C $min^{-1}$ with a Perkin Elmer TGA 7 instrument. DSC was conducted under nitrogen from 20 to 300 °C at a scan rate of 10 °C $min^{-1}$ with a Perkin Elmer Pyris 1 DSC instrument. Glass transition temperatures, $T_g$, correspond to inflection temperatures and liquid-crystalline/isotropic transition temperatures, $T_{lc/i}$, correspond to peak temperatures.

*Thin Films And Fibers*: Thin F8TBT films for microscopy and spectroscopy studies were spin-coated on glass substrates from homogeneous *o*DCB solutions (~20 g $L^{-1}$ F8TBT content) at ambient and, where applicable, thermally treated in a nitrogen-flushed Mettler FP82HT hot stage. Thin blend films (thickness ~80–100 nm) for microscopy, spectroscopy, and device studies were spin-coated from homogeneous *o*DCB solutions (~30–60 g $L^{-1}$ total material content; ratio of components 20:80 wt%:wt% F8TBT:$PC_{61}BM$) at ambient. F8TBT fibers were drawn from a chunk of **14** after swelling in chloroform.

*Optical Microscopy*: Optical microscopy was carried out with an Olympus BH2 polarising microscope. Thermal transitions of F8TBT were studied by heating/cooling thin films at a rate of 10 °C $min^{-1}$ in a nitrogen-flushed Mettler FP82HT hot stage.

*Scanning Force Microscopy (SFM)*: SFM was conducted with a Veeco Dimension 3100 system in tapping mode using Antimony (n) doped Silicon cantilevers (SCM-PIT, Veeco) with a force constant of 1–5 N $m^{-1}$, a resonance frequency of 60–100 kHz and a tip curvature radius of 20 nm.

*UV-vis Absorbance Spectroscopy*: Polarized UV-vis absorbance spectra of F8TBT and 20:80 F8TBT:$PC_{61}BM$ thin films as well as dilute *o*DCB solutions (0.1 g $L^{-1}$; quartz cuvette with 1 mm path length) were recorded using a Perkin Elmer Lambda 950 UV-vis spectrophotometer.

*Photoluminescence Spectroscopy*: A polarized photoluminescence emission spectrum of a F8TBT fiber, exited at 525 nm, was recorded through a linear polarizing filter using an Oriel liquid light guide and a Shamrock SR 303i spectrograph coupled to a Newton EMCCD silicon detector.

*Photovoltaic Devices*: Photovoltaic devices were fabricated on PEDOT:PSS coated (spin-coated from Baytron P, H. C. Stark GmbH, and treated at 150 °C for 30 min, thickness ~40 nm) patterned ITO-coated glass substrates. Blend active layers (film thickness ~80–100 nm; i.e., close to a thickness of 85 nm, at which the power absorption of such devices displays a local maximum [51]) were spin-coated as described above. A LiF electron-blocking layer (thickness ~6 Å) and aluminum top electrodes were deposited via thermal evaporation under vacuum (thickness ~80 nm; area ~4 $mm^2$).

Current density–voltage, *J*–*V*, characteristics were measured at ambient under simulated solar illumination (Air Mass 1.5, 1000 W $m^{-2}$). The light source used was a 300 Watt xenon arc lamp solar simulator (Photo Emission Tech.); the intensity was calibrated using a silicon photo-diode from Hamamatsu Photonics.

*FETs*: FETs were fabricated in bottom-gate bottom-contact configuration on highly doped silicon wafers with a thermally grown 100 nm silicon oxide layer; the two layers served as the gate electrode and gate insulator, respectively. Au source and drain electrodes, with a Cr adhesion layer were defined by standard photolithography (channel length, *L*, varied from 9 to 37 $\mu$m; width, *W*, varied from 2 to 16 mm to ensure a comparable *W*/*L* ratio and to exclude contact resistance effects). Blend active layers was spin-coated as described above.

Electronic characterization of FETs was conducted with a Keithley 4200 parameter analyzer in high vacuum. Saturation field-effect hole mobilities, $\mu_h$, were extracted from the transfer characteristics using

$$\mu_h = \left(\frac{\partial\sqrt{I_{sd}}}{\partial V_g}\right)^2 \frac{2L}{WC_i} \quad (1)$$

where $I_{sd}$ is the source-drain current (saturation regime), $V_g$ the gate voltage, $C_i$ the insulator capacitance, *W* and *L* the channel width and length.

## Acknowledgements

We acknowledge funding from the Northern European Innovative Energy Research Programme (N-INNER) as well as the Swedish Energy Agency through the projects Morphoso and Polarge.

Received: February 3, 2010
Revised: March 17, 2010
Published online: June 2, 2010

[1] Y. Ohmori, M. Uchida, K. Muro, K. Yoshino, *Jpn. J. Appl. Phys.* **1991**, *30*, L1941.
[2] M. Grell, D. D. C. Bradley, M. Inbasekaran, E. P. Woo, *Adv. Mater.* **1997**, *9*, 798.
[3] H. Sirringhaus, R. J. Wilson, R. H. Friend, M. Inbasekaran, W. Wu, E. P. Woo, M. Grell, D. D. C. Bradley, *Appl. Phys. Lett.* **2000**, *77*, 406.
[4] J. J. M. Halls, A. C. Arias, J. D. MacKenzie, W. Wu, M. Inbasekaran, E. P. Woo, R. H. Friend, *Adv. Mater.* **2000**, *12*, 498.
[5] R. Pacios, D. D. C. Bradley, J. Nelson, C. J. Brabec, *Synth. Met.* **2003**, *137*, 1469.
[6] M. Svensson, F. Zhang, S. C. Veenstra, W. J. H. Verhees, J. C. Hummelen, J. M. Kroon, O. Inganäs, M. R. Andersson, *Adv. Mater.* **2003**, *15*, 988.
[7] O. Inganäs, M. Svensson, F. Zhang, A. Gadisa, N. K. Persson, X. Wang, M. R. Andersson, *Appl. Phys. A* **2004**, *79*, 31.
[8] D. J. Brennan, P. H. Townsend, D. M. Welsh, M. G. Dibbs, J. M. Shaw, J. L. Miklovich, R. B. Boeke, A. C. Arias, L. Creswell, J. D. MacKenzie, C. Ramsdale, A. Menon, H. Sirringhaus, *Proc. SPIE* **2003**, *5217*, 1.
[9] C. L. Donley, J. Zaumseil, J. W. Andreasen, M. M. Nielsen, H. Sirringhaus, R. H. Friend, J.-S. Kim, *J. Am. Chem. Soc.* **2005**, *127*, 12890.
[10] R. Abbel, A. P. H. J. Schenning, E. W. Meijer, *Macromolecules* **2008**, *41*, 7497.
[11] D. J. D. Moet, M. Lenes, J. D. Kotlarski, S. C. Veenstra, J. Sweelssen, M. M. Koetse, B. de Boer, P. W. M. Blom, *Org. Electron.* **2009**, *10*, 1275.
[12] M. Grell, D. D. C. Bradley, G. Ungar, J. Hill, K. S. Whitehead, *Macromolecules* **1999**, *32*, 5810.
[13] G. Lieser, M. Oda, T. Miteva, A. Meisel, H.-G. Nothofer, U. Scherf, D. Neher, *Macromolecules* **2000**, *33*, 4490.
[14] M. Knaapila, R. Stepanyan, M. Torkkeli, B. P. Lyons, T. P. Ikonen, L. Almásy, J. P. Foreman, R. Serimaa, R. Güntner, U. Scherf, A. P. Monkman, *Phys. Rev. E* **2005**, *71*, 041802.
[15] M. J. Banach, R. H. Friend, H. Sirringhaus, *Macromolecules* **2003**, *36*, 2838.

[16] M. Knaapila, R. Stepanyan, B. P. Lyons, M. Torkkeli, T. P. A. Hase, R. Serimaa, R. Güntner, O. H. Seeck, U. Scherf, A. P. Monkman, *Macromolecules* **2005**, *38*, 2744.
[17] L. H. Sperling, *Introduction to Physical Polymer Science*, 2nd ed., Wiley, New York **2006**; p 113f.
[18] M. K. Kosmas, A. M. Kosmas, *Polymer* **1993**, *34*, 3115.
[19] F. Elias, S. M. Clarke, R. Peck, E. M. Terentjev, *Macromolecules* **2000**, *33*, 2060.
[20] T. G. Fox, P. J. Flory, *J. Appl. Phys.* **1950**, *21*, 581.
[21] P. J. Flory, *J. Am. Chem. Soc.* **1945**, *67*, 2048.
[22] V. Percec, M. Kawasumi, *Macromolecules* **1993**, *26*, 3663.
[23] H. Meier, U. Stalmach, H. Kolshorn, *Acta Polymer.* **1997**, *48*, 379.
[24] Y. Ding, A. Kisliuk, A. P. Sokolov, *Macromolecules* **2004**, *37*, 161.
[25] J. M. G. Cowie, *Eur. Polym. J.* **1975**, *11*, 297.
[26] J. Hintermeyer, A. Herrmann, R. Kahlau, C. Goiceanu, E. A. Rössler, *Macromolecules* **2008**, *41*, 9335.
[27] A. L. Agapov, A. P. Sokolov, *Macromolecules* **2009**, *42*, 2877.
[28] B. Tian, G. Zerbi, R. Schenk, K. Müllen, *J. Chem. Phys.* **1991**, *95*, 3191.
[29] D. Wasserberg, S. P. Dudek, S. C. J. Meskers, R. A. J. Janssen, *Chem. Phys. Lett.* **2005**, *411*, 273.
[30] K. G. Jespersen, W. J. D. Beenken, Y. Zaushitsyn, A. Yartsev, M. Andersson, T. Pullerits, V. Sundström, *J. Chem. Phys.* **2004**, *121*, 12613.
[31] K. Koynov, A. Bahtiar, T. Ahn, R. M. Cordeiro, H.-H. Hörhold, C. Bubeck, *Macromolecules* **2006**, *39*, 8692.
[32] L. M. Andersson, F. Zhang, O. Inganäs, *Appl. Phys. Lett.* **2007**, *91*, 071108.
[33] F. Zhang, K. G. Jespersen, C. Björström, M. Svensson, M. R. Andersson, V. Sundström, K. Magnusson, E. Moons, A. Yartsev, O. Inganäs, *Adv. Funct. Mater.* **2006**, *16*, 667.
[34] S. Nilsson, A. Bernasik, A. Budkowski, E. Moons, *Macromolecules* **2007**, *40*, 8291.
[35] C. M. Björström Svanström, J. Rysz, A. Bernasik, A. Budkowski, F. Zhang, O. Inganäs, M. R. Andersson, K. O. Magnusson, J. J. Benson-Smith, J. Nelson, E. Moons, *Adv. Mater.* **2009**, *21*, 4398.
[36] D. Veldman, Ö. İpek, S. C. J. Meskers, J. Sweelssen, M. M. Koetse, S. C. Veenstra, J. M. Kroon, S. S. van Bavel, J. Loos, R. A. J. Janssen, *J. Am. Chem. Soc.* **2008**, *130*, 7721.
[37] H. Aarnio, M. Westerling, R. Österbacka, M. Svensson, M. R. Andersson, H. Stubb, *Chem. Phys.* **2006**, *321*, 127.
[38] S. De, T. Kesti, M. Maiti, F. Zhang, O. Inganäs, A. Yartsev, T. Pascher, V. Sundström, *Chem. Phys.* **2008**, *350*, 14.
[39] A. Gadisa, M. Svensson, M. R. Andersson, O. Inganäs, *Appl. Phys. Lett.* **2004**, *84*, 1609.
[40] M. C. Scharber, D. Mühlbacher, M. Koppe, P. Denk, C. Waldauf, A. J. Heeger, C. J. Brabec, *Adv. Mater.* **2006**, *18*, 789.
[41] K. Vandewal, K. Tvingstedt, A. Gadisa, O. Inganäs, J. V. Manca, *Nat. Mater.* **2009**, *8*, 904.
[42] S. De, T. Pascher, M. Maiti, K. G. Jespersen, T. Kesti, F. Zhang, O. Inganäs, A. Yartsev, V. Sundström, *J. Am. Chem. Soc.* **2007**, *129*, 8466.
[43] C. Groves, R. A. Marsh, N. C. Greenham, *J. Chem. Phys.* **2008**, *129*, 114903.
[44] M. Lenes, M. Morana, C. J. Brabec, P. W. M. Blom, *Adv. Funct. Mater.* **2009**, *19*, 1106.
[45] L. J. A. Koster, V. D. Mihailetchi, P. W. M. Blom, *Appl. Phys. Lett.* **2006**, *88*, 052104.
[46] C. G. Shuttle, B. O'Regan, A. M. Ballantyne, J. Nelson, D. D. C. Bradley, J. R. Durrant, *Phys. Rev. B* **2008**, *78*, 113201.
[47] C. Deibel, T. Strobel, V. Dyakonov, *Phys. Rev. Lett.* **2009**, *103*, 036402.
[48] J. M. Frost, F. Cheynis, S. M. Tuladhar, J. Nelson, *Nano Lett.* **2006**, *6*, 1674.
[49] L. M. Andersson, F. Zhang, O. Inganäs, *Appl. Phys. Lett.* **2006**, *89*, 142111.
[50] A. M. Ballantyne, L. Chen, J. Dane, T. Hammant, F. M. Braun, M. Heeney, W. Duffy, I. McCulloch, D. D. C. Bradley, J. Nelson, *Adv. Funct. Mater.* **2008**, *18*, 2373.
[51] N.-K. Persson, H. Arwin, O. Inganäs, *J. Appl. Phys.* **2005**, *97*, 034503.